




Article

Fixed-Wing UAV Flight Operation under Harsh Weather Conditions: A Case Study in Livingston Island Glaciers, Antarctica

Ana Belén Bello ¹, Francisco Navarro ^{2,*}, Javier Raposo ³, Mónica Miranda ³, Arturo Zazo ²
and Marina Álvarez ¹

¹ ETS de Ingenieros Informáticos, Universidad Politécnica de Madrid, 28040 Madrid, Spain

² ETSI de Telecomunicación, Universidad Politécnica de Madrid, 28040 Madrid, Spain

³ ETS Arquitectura, Universidad Politécnica de Madrid, 28040 Madrid, Spain

* Correspondence: francisco.navarro@upm.es

Abstract: How do the weather conditions typical of the polar maritime glaciers in the western Antarctic Peninsula region affect flight operations of fixed-wing drones and how should these be adapted for a successful flight? We tried to answer this research question through a case study for Johnsons and Hurd glaciers, Livingston Island, using a fixed-wing RPAS, in particular, a Trimble UX5 UAV with electric pusher propeller by brushless 700 W motor, chosen for its ability to fly long distances and reach inaccessible areas. We also evaluated the accuracy of the point clouds and digital surface models (DSM) generated by aerial photogrammetry in our case study. The results were validated against ground control points taken by differential GNSS techniques, showing an accuracy of 0.16 ± 0.12 m in the vertical coordinate. Various hypotheses were proposed and flight-tested, based on variables affecting the flight operation and the data collection, namely, gusty winds, low temperatures, battery life, camera configuration, and snow reflectivity. We aim to provide some practical guidelines that can help other researchers using fixed-wing drones under climatic conditions similar to those of the South Shetland Islands. Performance of the drone under harsh weather conditions, the logistical considerations, and the amount of snow at the time of data collection are factors driving the necessary modifications from those of conventional flight operations. We make suggestions concerning wind speed and temperature limitations, and avoidance of sudden fog banks, aimed to improve the planning of flight operations. Finally, we make some suggestions for further research.

Keywords: Antarctica; glaciers; RPAS; UAS; flight operation; DSM; WMS; SDI



Citation: Bello, A.B.; Navarro, F.; Raposo, J.; Miranda, M.; Zazo, A.; Álvarez, M. Fixed-Wing UAV Flight Operation under Harsh Weather Conditions: A Case Study in Livingston Island Glaciers, Antarctica. *Drones* **2022**, *6*, 384. <https://doi.org/10.3390/drones6120384>

Academic Editors: Anna Zmarz, Rune Storvold and Osama Mustafa

Received: 3 November 2022

Accepted: 24 November 2022

Published: 28 November 2022

Publisher's Note: MDPI stays neutral with regard to jurisdictional claims in published maps and institutional affiliations.



Copyright: © 2022 by the authors. Licensee MDPI, Basel, Switzerland. This article is an open access article distributed under the terms and conditions of the Creative Commons Attribution (CC BY) license (<https://creativecommons.org/licenses/by/4.0/>).

1. Introduction

In the study of the evolution of glaciers under climate change, it is essential to count on accurate DSMs of the glaciers. Such models are required for glacier area and volume estimates, mass balance studies, and glacier dynamics modeling [1].

By the time of the data collection involved in this research (Antarctic campaign 2014/2015), many studies had been carried out using drones in the high Arctic [2] and mountain glacier areas such as the Himalayas [3–5] or the Italian Alps [6]. The bibliography available by that time on previous studies carried out using drones in Antarctica, mostly referred to the development of sensors [7,8] and their platforms [9,10], vegetation [11], fauna [12], and meteorological variables measurement [13,14], among others. They were seldom focused on the geometric modeling of the glacier surface, though some notable applications existed [15].

During recent years, and following the data collection for our study (2014/2015), there have been great technological advances in the world of drones, and most of such advances have been applied to Antarctic-focused research. A good compilation can be found in [16]. Such studies include development of flight platforms [17,18], use of positioning

systems (e.g., GNSS integration [19], RTK [20]), use and development of various sensors (LIDAR [21], multispectral [22], hyperspectral [23], thermal cameras [24,25]), use of different types of radar [26], monitoring volcanic gas emissions [27], monitoring fauna [28,29], and many more.

This article has been conceived and designed as a case study, using a Trimble UX5 UAV with an electric engine, focused on the behavior and operation of fixed-wing remotely piloted aircraft systems (RPAS) under the meteorological and logistical conditions typical of the South Shetland Islands, maritime Antarctica, which is described later. It aims to provide a practical account of our own experience in the use of fixed-wing RPAS in such an environment, which will be helpful to other researchers using similar platforms under comparable climatic conditions. It can serve as a guide to improve the planning of flight operations, including the replacement of drone elements that may hinder operations, as well as helping to prevent possible problems, perhaps unforeseen, associated to the behavior of the aircraft and its cameras under extreme weather conditions.

With such an aim, various hypotheses are proposed and tested, based on the main variables that can affect the flight operations (aircraft stability in flight under gusty winds, behavior of the drone's materials at low temperatures, battery life, camera configuration to reduce the effects of albedo, etc.). We wish to emphasize that our study does not aim to be a comparison of fixed-wing versus multirotor systems. The latter have also been shown to provide excellent results in the Antarctic environment (e.g., [15]). Neither do we pretend that our study pioneers the use of fixed-wing RPAS in environments such as the South Shetland Islands, as there are some notable examples (e.g., [30]). Our commitment to the analysis of the flight operations of fixed-wing RPAS in harsh environments such as those present on Livingston Island is based on desirable properties of such aircraft, which is analyzed later, supported by previous applications [30].

Another objective of our research is to analyze the accuracy of the point clouds and digital surface models (DSM) generated by aerial photogrammetry from the captured flight data, and determine their usefulness for glacier dynamics studies [31]. This was performed by validating the data extracted from the DSM against ground control points (GCP) taken in situ using GNSS techniques.

Finally, we set as an additional objective that the results obtained in this research are shared through web publication of the DSM and all the derived maps generated from them. This was done following the Open Geospatial Consortium (OGC) standards [32] and European, Spanish, and global specifications (IDEE [33], INSPIRE [34], and ISO [35], respectively) to create a prototype of Spanish spatial data infrastructure (SDI) in Antarctica.

In summary, the contribution of the present study to broadly available literature is to provide some practical hints on how to operate a fixed-wing RPAS under polar maritime climate conditions. This is achieved by optimizing operation planning (flight coverage, analysis of meteorological conditions and risks), selecting flight parameters (flight height, camera configuration, etc.) according to the weather forecast and its possible effects on the flight operations (aircraft stability under gusty winds, icings, albedo effects on optical images, etc.), and by carrying out the planned flight under safe conditions. All of this effort is orientated to minimize the risks involved in such flight operations, aiming to obtain the maximum benefit from the fieldwork carried out.

2. Study Site

Our investigation focused on Livingston Island, the second largest island of the South Shetland Island archipelago, where the Spanish Antarctic Station Juan Carlos I (BAE JCI, using its Spanish acronym) is located (Figure 1). This station provided the logistic support to our fieldwork. These islands are located close to the northwestern coast of the Antarctic Peninsula and are characterized by low-pressure systems with prevailing westerly winds, implying wet and windy conditions. Although the mean annual temperatures are not extremely low, the presence of humidity facilitates the appearance of icings.

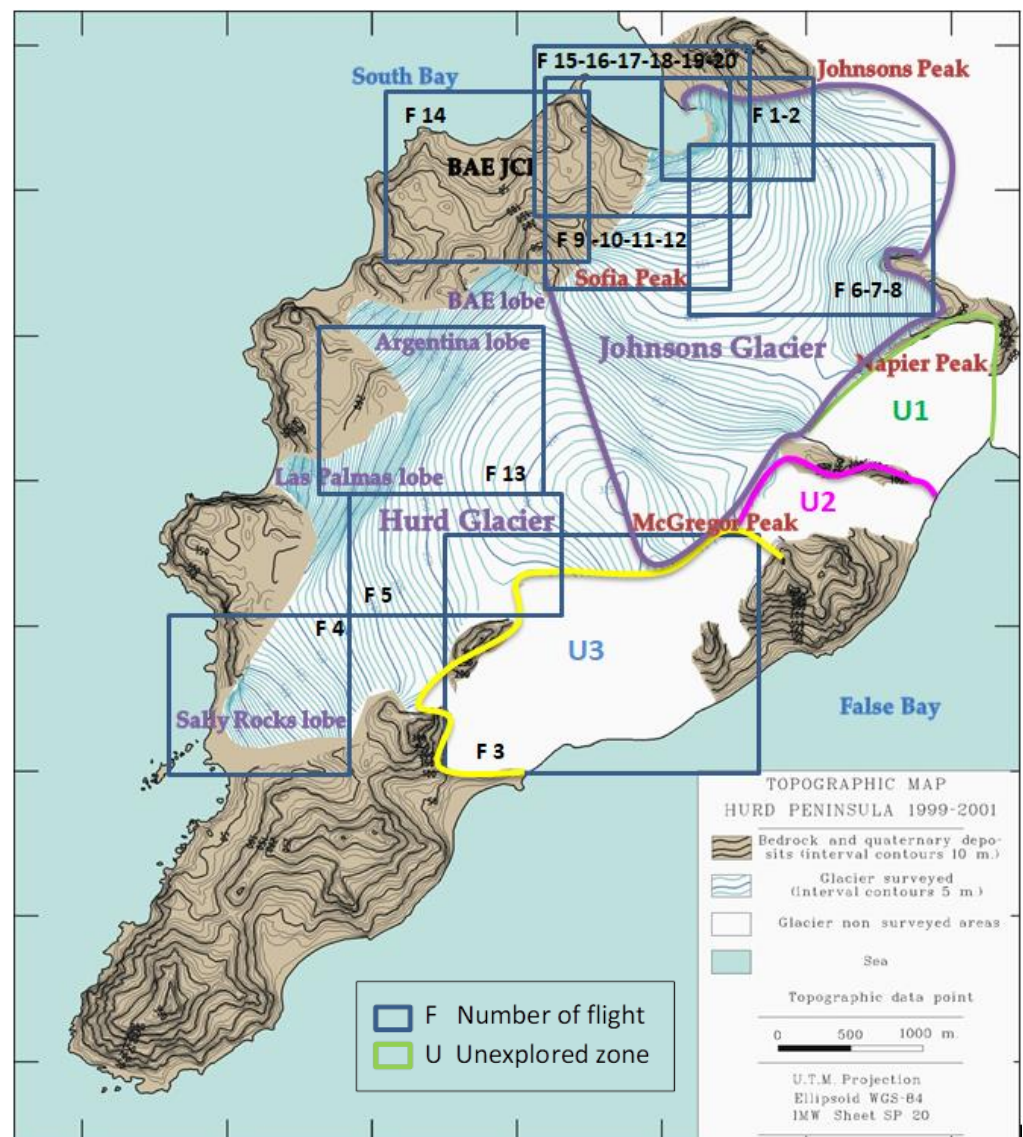


Figure 1. Study site, showing the main geographical features of Hurd Peninsula, Livingston Island, and the planned flight areas (source: authors).

The glaciers under study are situated on Hurd Peninsula (28 km²) and cover an area of approximately 11 km². Two main glacier units can be identified: Johnsons Glacier, 5.6 km² in area, which is sea-terminating, and Hurd Glacier, with an area of 3.6 km², which terminates on land (Figure 1). The latter has four main tongues (or lobes), named BAE, Argentina, Las Palmas, and Sally Rocks. These two glaciers span an altitude ranging from sea level to ca. 330 m a.s.l.

The climatic conditions at BAE JCI and at an automatic weather station on Johnsons Glacier are shown in Table 1. Such variables are critical for RPAS flight operations.

Table 1. Summer weather statistics at JCI station (1987/88–2013/14) and on Johnsons Glacier (2006/07–2013/14) (source: [36]).

Summer Statistics	BAE JCI	Johnsons
Mean temperature (°C)	1.9	0.2
Max temperature (°C)	15.5	11.0
Min temperature (°C)	−7.0	−11.6
Relative humidity (%)	80	
Precipitation (mm)	148.6	
Mean pressure (hPa)	987	
Max pressure (hPa)	1017.6	
Min pressure (hPa)	898	
Mean wind speed (km/h)	12	16
Max wind speed (km/h)	138	134

3. Materials and Methods

3.1. Preliminary Considerations: Choice of the Drone

The first study, prior to the trip to Antarctica, was to establish which would be the unmanned aerial system (UAS) to fly under the harsh meteorological conditions of the work area. The characteristics of the glaciers involved (extension, orientation, zones of steep relief, etc.), together with the logistic limitations on Livingston Island, also had to be taken into account. We carried out an analysis of the local climate, based on the reports published by the Spanish Meteorological Agency (AEMET) [36]. From this analysis, we concluded that the determining variables for the quality of the results were air temperature, relative humidity, atmospheric pressure, precipitation, wind speed and direction, insolation, and albedo.

These variables affected different UAS elements and their functioning and conditioning of the aircraft behavior. A matter of particular concern was the occurrence of strong and gusty winds, which are a very frequent meteorological phenomenon on these islands [36]. Accordingly, we gave special attention to the effects on the aircraft trajectory by wind [37]. The general rule of thumb for flying drones is that the wind speed should be no more than two-thirds of the maximum speed of the drone. It has also to be borne in mind that the higher the wind speed, the greater the consumption of battery power. We established as a prerequisite regarding battery life that it should last for at least 45 min, to allow flying over large open areas. Owing to the logistical limitations when working on glaciers and the associated safety regulations of BAE JCI, movements on the glaciers had to be kept to a minimum (see an exemplary illustration in Figure 2), and it was therefore desirable to be able to cover the largest possible surface from a single, safe takeoff position, and to travel long distances in BVLOS flight. Battery life was also important in this context, to allow for the maximum flight distance (round trip) without having to change position and do multiple flights. All of these conditioning factors were analyzed, taking into account the types of drones existing in the market in 2014, and also their availability. Such drones are classified in many articles according to their operational characteristics [38,39]. An aircraft with stability in flight, long autonomy, and resistance to gusty flights was required. The system should also withstand rapid temperature changes, without being affected by adiabatic currents, by snow or rain precipitation, or by fog. A fixed-wing RPAS seemed advisable (as compared with a multicopter system), since its flight operations are best suited for working on open and extensive areas, being capable to cover more surface in less time. Moreover, they respond better under strong and gusty winds.

For our investigation, a Trimble UX5 RPAS [40] (fixed-wing RPAS of the microdrone-type) with an electric engine was available. It carries a Sony NEX-5 metric camera with fixed focal length (15 mm), 24 Mpx APSC sensor type, and Voigtländer lenses [41]. This fixed-wing RPAS complied a priori with the requirements stated above, according to the technical and operational specifications shown in Table 2 and the operational limitations summarized in Table 3.

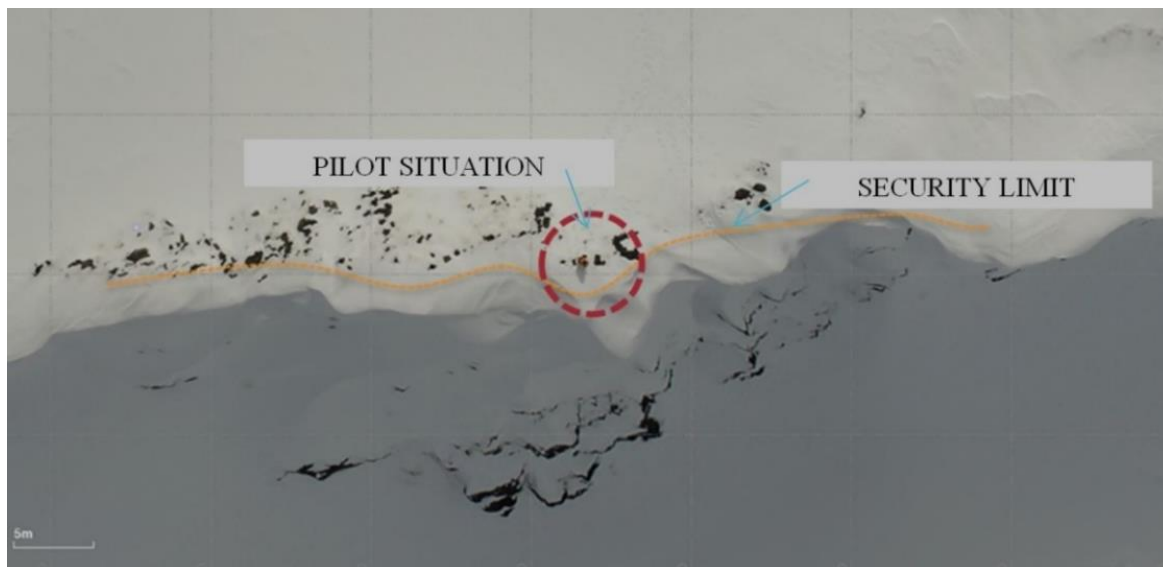


Figure 2. An illustration of safety limitations on the pilot's situation imposed by the presence of crevasses.

Table 2. Technical and operational specifications for Trimble UX5.

Technical Specifications	
Weight	2.5 kg (5.51 lb)
Dimensions	100 cm × 65 cm × 10.5 cm (39.37 in × 25.59 in × 4.13 in)
Material	EPP foam; carbon frame structure; composite elements
Propulsion	Electric pusher propeller; brushless 700 W motor
Battery	14.8 V, 6000 mAh
Operational Specifications	
Endurance	50 min
Range	60 km (37.28 mi)
Cruise speed	80 km/h (50 mph)
Maximum ceiling	5000 m (16,404 ft)
Takeoff Type	Catapult launch
Landing Type	Belly landing
Weather limit	65 km/h (40.39 mph) and light rain
Communication and control frequency	2.4 GHz (FHSS)
Communication and control range	Up to 5 km (3.10 mi)

Table 3. Operational limitations for Trimble UX5.

Condition	Acceptable RANGE
Weather limitations	Light rain is acceptable; avoid hail, snow, and heavy showers
Head wind (for cruise flight)	Maximum 55 kph (34 mph)
Cross wind:	
For takeoff/landing	Maximum 30 kph (19 mph)
For cruise flight	Maximum 55 kph (34 mph)
Gusts (for cruise flight)	Maximum 15 kph (9 mph)
Turbulence	Avoid turbulence at all times
Temperature:	
Rover, including eBox and gBox	−20 to +45 °C (−4 to 113 °F)
Camera *	0 to +30 °C (32 to 86 °F)
Battery *	0 to +30 °C (32 to 86 °F)
Launcher *	+10 to 45 °C (50 to 113 °F)

* Preflight conditioned temperature.

3.2. Working Hypotheses

Based on the considerations presented in the previous subsection, different hypotheses were proposed for testing, through our case study:

1. **Stability of the aircraft in flight under gusty winds:** Setting the stability hypothesis was based on the technical characteristics of the aircraft, stating that the aircraft could withstand lateral winds of up to 50 km/h and gusty winds of up to 15 km/h with a cruise speed of 80 km/h [42]. Therefore, the initial hypothesis was that it could fly with winds less than 50 km/h, and its alternative hypothesis that it could not withstand winds greater than or equal to 50 km/h.
2. **Battery life:** There are previously published studies regarding the decrease in battery life under low temperatures [43]. Therefore, it was anticipated that this effect would occur when flying the RPAS in Antarctica. The unknown to be resolved was the magnitude of this decrease, so the initial hypothesis was set as follows: battery life decreases less than 30%; and its alternative as follows: battery life decreases more than 30%. If the second hypothesis was confirmed, it would not be possible to fly safely, since a minimum reserve of 15% is required.
3. **Behavior of the drone materials:** The behavior of the materials comprising our UAS at low temperatures was unknown, not even the technical specifications made reference to it. The main materials were high-density polyethylene foam and carbon fiber frame structure and composite elements. Accessory elements, such as the shuttle, also had to be taken into account. The initial hypothesis was that none of these materials would be severely affected, and its alternative hypothesis that some of them could fail.
4. **Metric camera configuration:** There are various studies on the reflectance of snow and how it affects photographs, including aerial ones [44]. A study was needed on how to reduce such undesirable effects to obtain images of sufficient quality to produce a solution after image correlation. We started from the hypothesis that good results would be obtained with the adjustments proposed by the manufacturer. If this hypothesis were not corroborated, a manual configuration would be used.
5. **Aircraft's ability to fly very long distances:** There were some unexplored areas that had not yet been surveyed in previous field campaigns (U1, U2, and U3 in Figure 1). Problems faced here were how to access safely these areas with the available logistics, and estimating a priori the distance that the plane could fly over them. The initial hypothesis raised was based on the drone's technical characteristics. These indicated that, assuming good battery conditions, the aircraft could travel 60 km in 50 min, reserving 5 min for takeoff and another 5 min for landing. The possibility of varying the flight height to fly over the largest possible surface, with the required precision, was also considered.

3.3. Software Tools

To attain the various objectives established in this research, various methodologies were implemented in our case study, using diverse software (Table 4).

Table 4. Summary of objectives, associated techniques and methods, and computer tools.

Objectives	Techniques and Methods	Software Used
Adaptation of aerial photogrammetry using drones to Antarctic weather conditions	- Study of Antarctica weather conditions - Adaptation of flight operations - Capture and analysis of data	- Trimble Aerial Imagine [45] - Trimble Access [46] - Trimble Business Center (TBC) [47]
Generation of DSM of glaciers and derived cartography	- Obtaining point cloud - Data processing and analysis - Generation of DSM	- TBC - ArcGIS 10.1 [48]
Web publication of results as a prototype of Antarctic SDI	- Publication of generated cartography - Configuration for WMS	- PostGIS [49] - Geoserver [50]

3.4. Flight Operations

The ideal flight conditions are sunny days, without precipitation or fog, and without very strong winds. Such ideal conditions are rarely met in an environment such as our study site. For planning the flights, we had available the daily weather forecasts from both AEMET and the European Centre for Medium-Range Weather Forecasts (ECMWF), showing the amount of clouds, relative humidity, precipitation, atmospheric pressure, wind speed and gusts, and temperature (see an example in Figure 3). To plan and monitor the flights, we had available the Trimble Access Aerial Imaging software [45], which plans the project, performs prechecks and monitors the flight, and the Trimble Business Center software with photogrammetry module [47], used for both planning purposes (e.g., data capture) and for processing the aerial images and creating the final cartographic products.

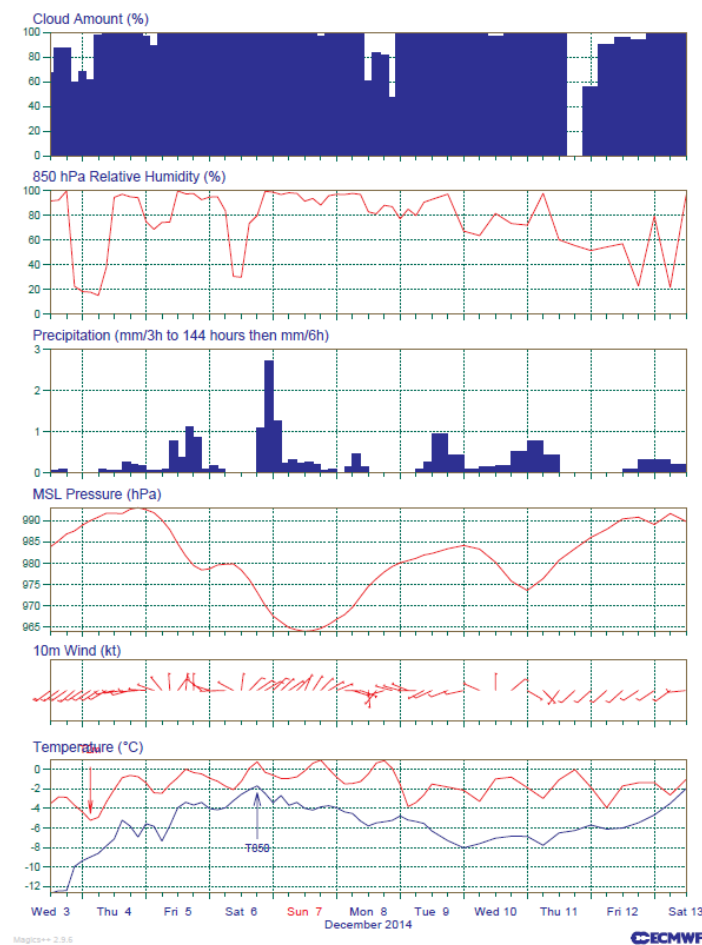


Figure 3. Forecast from 2 to 12 December for 62.62° S 60.3° W (source: ECMWF).

In total, 20 flights were made (Table 5). Although our stay at BAE JCI began on 1 December 2014 (dd/mm/aa), the flights could not begin until 4 December 2014 due to the tasks related to the station opening and the startup of work equipment and communication systems (BAE JCI is only operated during the austral summer season). In addition to technical and weather condition issues discussed earlier, logistic considerations had also to be taken into account, including the availability of mountain guides to support our safe work on the glaciers, the time needed to reach the takeoff position on the glacier, and the difficulties inherent to move across the glacier because of the presence of crevasses (e.g., Figure 2). As mentioned, this motivated the flights to be planned from a single takeoff and landing position, trying to cover the maximum possible surface with a single flight. Taking into account these factors, together with those related to weather conditions, resulted in that only 7 out of 20 days of stay at the base could be used for flights.

Table 5. Summary of the flights carried out and their characteristics.

Flight ID	Date (yyymmdd)	Location	Flight Time (hh:mm)	Flight Duration (hh:mm)	Flight Height (m)	GPS Nr. Satellites	Weather Type	Temp (°C)	Wind Speed (kt)	Wind Direction	Camera Configuration	Nr. Photos	GSD (cm)
1	141204	Johnsons Glacier		0:12	300	10	fog	[−4, −3]			(S) 5.6 1/2000 ISO AUTO	104	9.6
2	141204	Johnsons Glacier& Johnsons Peak		0:05		10	fog	[−4, −3]			Internal Video	-	-
3	141206	Glacier (Mac Gregor)		0:33	210	11	sunny	[−4, −3]		NNE	(S) 5.6 1/2000 ISO AUTO	140	6.7
4	141206	Sally Rocks Glacier (Up)		0:01	250	11	sunny	[−4, −3]			(S) 5.6 1/2000 ISO AUTO	-	6.7
5	141206	Hurd Glacier (test2)	13:01	0:40	100	11	sunny	[−4, −3]			(S) 5.6 1/2000 ISO AUTO	834	3.2
6	141209	Johnsons Glacier&Flight1	14:30	0:40	150	11	cloudy	[−4, −3]	15–20	SW	(A) 9 1/4000 ISO 100	160	4.8
7	141209	Johnsons Glacier&Flight2_Video	16:17	0:30	150	11	cloudy	[−4, −3]	15–20	SW	Internal Video	-	-
8	141209	Johnsons Glacier&Flight3	16:47	0:35	75	11	cloudy	[−4, −3]	15–20	SW	(A) 9 1/4000 ISO 100	67	2.4
9	141213	Johnsons Glacier & Bay(RGB)	11:00	0:01	260	11	overcast	[0, 1]	0–5	SSE	(S) 5.6 1/4000 ISO 100	-	8.0
10	141213	Johnsons Glacier_Cross Bay	11:15	0:32	260	12	overcast	[0, 1]	0–5	SSE	(S) 5.6 1/4000 ISO 100	458	8.0
11	141213	Johnsons Glacier_Sofia Peak (RGB)	12:00	0:32	260	12	overcast	[0, 1]	0–5	SSE	(S) 5.6 1/4000 ISO 100	204	8.0
12	141213	Johnsons Glacier_Sofia Peak (RGNir)		0:01	260	12	overcast	[0, 1]	0–5	SSE	(S) 5.6 1/4000 ISO AUTO	-	-
13	141216	Hurd Glacier		0:02	150	12	sunny	[0, 1]	0–5	SSE	(S) 4.5 1/4000 ISO AUTO	234	4.8
14	141219	BAE Juan Carlos I (BAE JCI)	16:45	0:15	75	11	cloudy	[0, 1]	05–10	NE	(S) 4.5 1/4000 ISO AUTO	23	2.4
15	141220	Johnsons Glacier (Diff. Heights)	11:08	0:05	150	12	cloudy	[0, 1]	05–10	NE	(S) 4.5 1/4000 ISO AUTO	-	4.8
16	141220	Johnsons Glacier (Diff. Heights_2)	11:35	0:05	150	12	cloudy	[0, 1]	05–10	NE	(S) 4.5 1/4000 ISO AUTO	-	4.8
17	141220	Johnsons Glacier (Diff. Heights_3)	12:03	0:21	150	12	cloudy	[0, 1]	05–10	NE	(S) 4.5 1/4000 ISO AUTO	214	4.8
18	141220	Johnsons Glacier (Diff. Heights_4)	12:54	0:17	260	12	cloudy	[0, 1]	05–10	NE	(S) 4.5 1/4000 ISO AUTO	104	4.8
19	141220	Johnsons Glacier_Cross Bay_2	13:54	0:38	260	11	cloudy	[0, 1]	05–10	NE	(S) 4.5 1/4000 ISO AUTO	512	4.8
20	141220	Johnsons Glacier (RGNir)	14:40	0:21	260	9	cloudy	[0, 1]	05–10	NE	(S) 4.5 1/4000 ISO AUTO	104	-

As can be seen in Table 5, the duration of the flights was in all cases below 40 min. We found that the duration of the batteries was reduced by 30% due to cold conditions, as proposed in the first hypothesis, and it was necessary to leave 5 min of reserve for the return of the aircraft.

The parameters used in the first flights were those recommended by the camera manufacturer: an aperture of 5.6 and a speed of 1/2000 with automatic ISO. The coordinate system used for capturing geospatial information for all flights was the WGS84 UTM projection on the 20 South sheet.

Flights 1 and 2 were made on 4 December 2014 and were test flights. The first one, using the RGB camera, lasted just 12 min due to the risk of fog. We had no previous experience in flying under such conditions. In fact, in the second flight, the fog fell and the plane crashed shortly after takeoff. The reason is that, due to the low temperatures, the fog is formed by ice crystals, which cause Pitot tube obstruction and airframe gelation.

Flights 3, 4, and 5 were flights made on 6 December 2014 with the standard camera specifications, with sunny weather, and with temperatures on the ground of $-4\text{ }^{\circ}\text{C}$ (temperatures a few degrees lower have to be considered at flight height). Flight 3 was made over McGregor Peak, attempting to map the unexplored area U3 (Figure 1). The pilot canceled this flight after 33 min because the trajectory of the plane did not follow the planned route according to the cartography used as the basis for flight planning. The reason was that this cartography was published with an error in the magnetic declination, due to a change in east–west orientation. This required that in situ transformations of the existing cartography had to be carried out. A video of this flight and its problems can be seen in [51].

The fourth flight was planned over the Sally Rocks lobe of the Hurd Glacier, but the aircraft did not takeoff with sufficient speed due to lack of tension in the shuttle tires. The reason is that low temperatures cause a decrease in the elasticity of the tires. When launching the airframe with its payload, the elastic inside pulls the launch dock with more than 4g and with a speed of more than 60 km/h. To maintain this performance with temperatures below 0–10 $^{\circ}\text{C}$, it is necessary to increase by at least 25% the standard elastic tension. For this reason, the manufacturer recommends keeping the launcher as warm as possible and covering it immediately after the plane has been launched. This was carried out for the other flights. In the fifth flight, the height was modified to check which would be the adequate flight height to obtain the precision established a priori and to cover the entire extension of the glaciers in the shortest possible time. The flight was unfolded over the Hurd Glacier without any further setbacks. Photographs taken by the RPAS on sunny days were reviewed, and the images were found to be very dark but sharp. So it was considered to vary the parameters of the camera, since the exposure time had been prioritized in the previous flights.

Flights 6, 7, and 8 were performed under cloudy weather, which recommended changing the camera settings to an f-stop between 8 and 11, letting the exposure time to be calculated automatically, and with an ISO of 100. Priority was given to the aperture, to change the focus range and background blur. A low blur value sharpens the foreground, and a high blur sharpens the background. This setup did not work out very well, so another variation in parameters for the last few flights was tried: an aperture of 4.5 and a speed of 1/4000 with automatic ISO, which gave better results. Flight 7 was a video recording flight, and Flight 8 was made changing the flight altitude. The precision that can be achieved in the point cloud depends on the flight altitude. Until the flight zone is accessed and the surrounding terrain is observed, it is not possible to confirm how high it is possible to fly. As can be seen in Table 5, different heights were set on different flights for the mentioned reasons, resulting in different ground sample distances (GSDs). All the accuracies obtained were below the precision of the existing cartography.

Flights 9, 10, 11, and 12 were carried out on 13 December 2014 over Sophia Peak and Johnsons Glacier at the same flight height, with overcast skies, little wind, and a ground temperature of 0 $^{\circ}\text{C}$ (again, a few degrees lower at flight height). This prompted changing the shutter speed from 1/2000 to 1/4000 and the ISO from auto to 100. In the ninth flight,

the takeoff failed due to either lack of sufficient wind to sustain the aircraft in flight or to lack of sufficient tension in the rubber bands, causing them to stick, or both reasons together. The twelfth flight was planned with an RGNir camera, but it was not carried out because the takeoff failed again.

Flight 13 (16 December 2014) was planned over Hurd Glacier with the same configuration, in a sunny day, but changing the lens aperture from 5.6 to 4.5 and the flight height to 150 m. However, two minutes after takeoff, an emergency landing (FES) had to be made because communications with the UAV were lost.

In flight 14 (19 December 2014), over Juan Carlos I Station, the same camera configuration was maintained, but the flight height was changed to 75 m above ground level, because the flight had to be more precise to observe the ground control points (GCP) located close to sea level.

On the last day with conditions suitable to fly (20 December 2014), various flights (15, 16, 17, 18, 19, and 20) were made over the same glacier (Johnsons), changing the flight heights and maintaining the same camera configuration, which had shown to be the most appropriate. In the first two, communication between the plane and the controller was lost, which forced us to anticipate the landing. The weather was cloudy with little wind.

Of the twenty-five days that the RPAS was available at the Antarctic station, only seven days could be flown, due to adverse weather conditions, mainly wind gusts exceeding 60 km/h, snow storms, fog that obstructed the aircraft's Pitot tube, and very low temperatures at flight height, which caused icings on the wings of the RPAS. Logistic problems also played a relevant role, due to the time required to reach the glaciers, to check the drone's materials and to initiate the flight. The reduction in the duration of the flight due to the shorter duration of the batteries under cold conditions, as well as the fact that not all rescue and emergency means were readily available (because the field campaign had just started) imposed further limitations.

3.5. Data Processing

Once all the flight data and images were available, processing was carried out using the TBC software [47] to obtain an adjusted point cloud of the study area. With this aim, the images were first processed, together with the aircraft's navigation information, following the standard method of photogrammetry (internal, relative, and absolute orientation) [52].

Overall, the computations involved in the processing of the flight data were less extensive than expected, as was the glacier coverage. The conditioning factors, already explained, about the difficulties in the logistics of access to the glaciers, the reduction in the duration of the batteries due to the cold conditions and, above all, the reflectivity of the snow, made the surface flown smaller than initially planned. Furthermore, it was not possible to extend the survey to unexplored areas.

Figure 4 illustrates the share of the surface surveyed in flight F13 (the whole rectangle shown) for which we could obtain image correlation (the yellow area) after filtering the images. The reason was that, because of the reflectivity of the snow, there was a lack of contrast between the photographs, necessary for the software to identify the same pixels in contiguous images. We tried to reduce this lack of contrast for the subsequent flight operations by reconfiguring the camera and by generating "artificial" contrasts on the glacier surface. The latter was done by deeply marking the tracks of the snowmobiles. The subsequent adjustment of the flight gave standard deviations of 3 cm in planimetry and 6 cm in altimetry for the resolved area, which was within the tolerance established a priori.

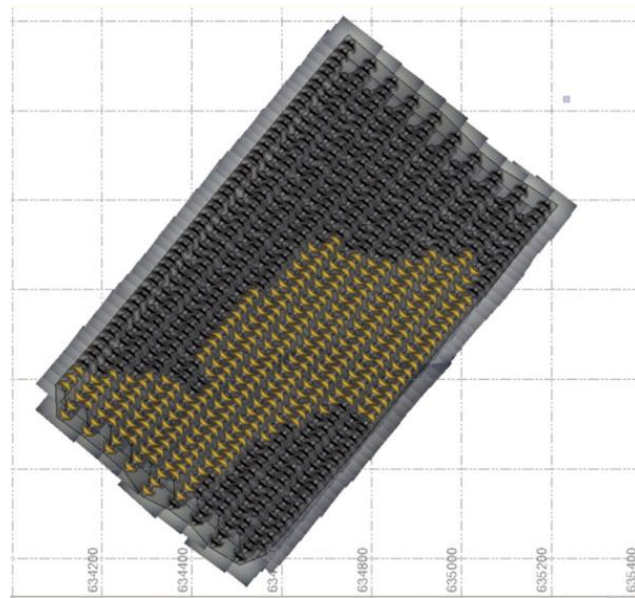


Figure 4. Captured (all) and processed (yellow) images for flight F13 (see Figure 1) over Hurd Glacier.

Subsequently, segmentation and filtering algorithms were applied to lighten the amount of information and to clean the noise generated by the albedo, as can be seen in Figure 5a. Data were resampled at distances of 3 m (Figure 5b) in order to generate a more manageable DSM. The pixels were also classified as terrain or nonterrain to eliminate outliers in the form of points with unusually high (and out-of-range) elevation, and to be able to generate smoother models.

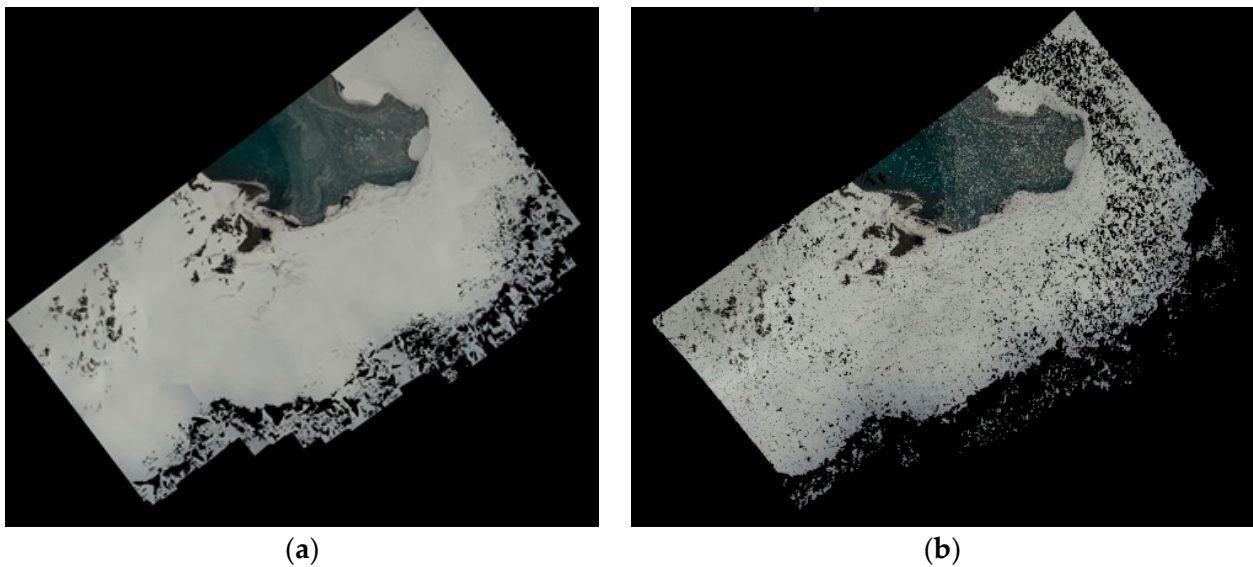


Figure 5. (a) Original point cloud and (b) point cloud resampled at 3 m.

A geostatistical analysis of the generated point clouds was carried out to verify the quality of the data and to validate them for the generation of the DSM.

3.6. Modeling the Glacier Surface

TBC software was used to generate the digital elevation models (DEM). In the first set of results generated, it was observed that the models were very rough, due to the noise caused by the reflectivity of the snow, even if it had already been reduced in the point clouds by the application of various filters.

Therefore, an analysis was carried out using different programs (ArcMap [48], GRASS [53], and TBC), aiming to improve these results by means of different algorithms [54]. As a conclusion of the study, it can be stated that the TBC triangulation loses triangles when grouping points that share the same height (Z axis), while ArcMap and GRASS do not, so their resulting surface appears more abrupt. Regardless, none of the mentioned software packages managed properly the spikes resulting from the snow reflectivity, so other possibilities for modeling surfaces were tested.

A trial was used to generate a digital terrain model (DTM) instead of a DSM (Figure 6a). In the former case, classification algorithms are used to determine out-of-range elevations and to assign terrain or nonterrain characteristics to each point [48]. The classification algorithms of TBC software were applied and the results improved, eliminating part of the spikes, without affecting the image quality, generating a smoothed surface with reduced noise generated by snow reflectivity (Figure 6b).

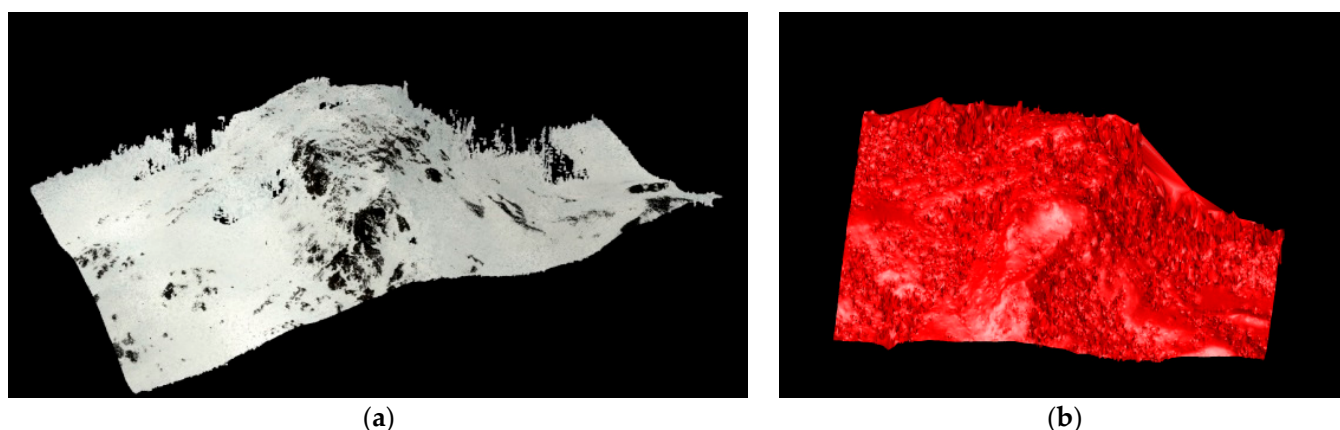


Figure 6. (a) DSM and (b) DTM of Sophia Peak.

To validate the obtained DTMs, we compared the model results with the ground control points, which provided an estimate of the spatial accuracy of our results. These GCPs were taken in the field using GNSS techniques and were not used in the adjustment of the point cloud. In other words, calibration and validation points were separate sets of data. These GCPs were projected onto the DTM and the differences were observed. The results of this comparison are presented in the corresponding section.

After the generation of the glacier DSM, various derived maps were generated for use in different applications on glacier dynamics and mass balance studies. These derived maps were generated using two different software packages: TBC for the generation of the orthoimages and DTMs, and ArcGIS to generate other derived maps such as maps of slopes, orientations, and contour lines.

3.7. Web Publication and Prototype of Antarctic Space Data Infrastructure (SDI)

Another objective of this research was to make our results available to the scientific community by publishing them through a web server. This was performed in compliance with OGC standards and Spanish, European, and worldwide specifications (IDEE, INSPIRE, and ISO, respectively) to create a prototype of a Spanish spatial data infrastructure (SDI) in Antarctica. DTM and derived maps were generated in GeoTIF format [55], and were then exported to a database (DB) for storage and management, in this case, PostGIS [49]. All data were imported into the PostGIS database, transformed from other formats such as GML, GeoJSON [56], or LandXML [57], depending on its origin. With Geoserver [50], the web map service (WMS) was created for its publication and management through a geographic information system (GIS). A WMS is a web mapping service that allows SDI images and data to be shared, queried, and exported on the web, using the OGC protocol. The integration of GIS with Geoserver allows, when publishing the models of an SDI, to directly select a table from the DB as a data source for the WMS. It also allows the images

and data of the SDI to be shared, consulted, and exported on the web, using the OGC protocol (Figure 7).

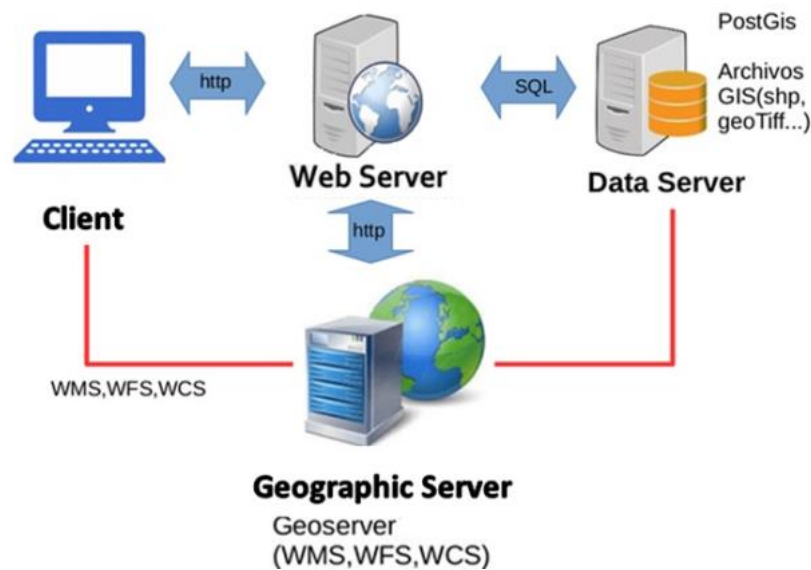


Figure 7. Web mapping structure (source: ESRI).

Geoserver is a very simple tool that allows creating a WMS service to publish and manage GIS data exchange services quickly and without difficulties. Developing the WMS involves following a series of steps: environment installation, workspace configuration, configuring PostGIS as a data source, creating a layer in GeoServer, specifying layer settings, and previewing the generated maps. The necessary parameters and metadata must be configured for the WMS service. The limited SRS (spatial reference system) list is populated with the reference system of the models and maps to be published. EPSG (European Petroleum Survey Group) codes are used. All these configuration parameters can be seen in the so-called capabilities file.

PostGIS is configured as the data source and a connection is created between GeoServer and the PostGIS database, where the data of the models are stored. A GETMAP request, in URL format [58], must be made to the WMS, either through a “thick” client such as ArcGIS, GVSIG, or Google Earth, or through a “thin” client such as Leaflet or OpenLayers [59]. Finally, the name of the layer to show and the format with which the layer is opened, in this case OpenLayers, are selected.

4. Results

As described in the methods section, different hypotheses were raised regarding the behavior of the flight system used, a fixed-wing RPAS Trimble UX5 with electric engine, which were verified through our case study.

The following results were obtained from the experiments carried out:

1. As already explained in Section 3.1, the main impediment to flight operations was the wind, together with precipitation. Wind remained constant at typical speeds of 10–15 km/h, reaching peaks of up to 65–100 km/h on some days. An example can be seen in [60]. This limited the actual number of days of flight to 7 out of 20 possible days (gray columns in Table 6).

Table 6. Summary of weather forecasts for Livingston Island during the period of the measurements. Data extracted from AEMET and ECMWF weather forecasts.

Date (dd/mm/yyyy)	2 December 2014	3 December 2014	4 December 2014	5 December 2014	6 December 2014		7 December 2014	8 December 2014	9 December 2014	10 December 2014
Cloud cover	overcast	cloudless	fog	overcast	sunny		cloudy	cloudy	cloudy	cloudy
Rainfall/Snowfall	yes	no	no	yes	no		yes	yes	no	yes
Wind (km/h)	20	28	10	35	25		15	20	35	40
Gust (km/h)	45	38	25	45	35		25	25	65	100
Date (dd/mm/yyyy)	11 December 2014	12 December 2014	13 December 2014	14 December 2014	15 December 2014	16 December 2014	17 December 2014	18 December 2014	19 December 2014	20 December 2014
Cloud cover	cloudy	cloudless	cloudless	cloudy	cloudy	sunny	cloudy	cloudy	cloudy	cloudy
Rainfall/Snowfall	yes	no	no	yes	yes	no	yes	yes	no	no
Wind (km/h)	40	30	10	25	25	35	30	40	20	20
Gust (km/h)	65	55	25	35	35	45	45	55	25	25

In the worst scenario, the plane was able to fly with constant winds of up to 35 km/h, withstanding gusts of 65 km/h (see also Tables 2 and 3). A graphical illustration of such windy conditions can be found in [61].

The flight time had to be shortened, thus reducing the extension of the area covered by the flight, due to the low temperatures, which limited the duration of the batteries. As already explained, the journey to the glaciers entailed time and risk due to crevasses, sometimes hidden by snow bridges. The time windows of favorable weather conditions were not very long, so the planning had to be very tight and with as few flights as possible, each covering the largest possible area. This implied that flights had to be planned with a reserve of 30%, instead of the usual 10%. Table 7 shows the reduction in coverage (km²) and number of flight lines derived from a 30% reduction in battery life. Taking into account that the UAV has a range of 60 km with a 100% battery charge, this range becomes 42 km with a 30% reduction in battery life (21 km for each section of a round trip). This amount can be further reduced based on the flight height, due to the colder conditions at higher altitudes. Such calculations were made using the flight planning software, Trimble Access, so that, by selecting the flight zone and battery reserve, the safe takeoff zone could be selected (Figure 8).

Table 7. Comparison of coverage with full and reduced battery level.

Battery Level 100%				Battery Level Reduced 30%			
Height	GSD (cm)	Coverage (km ²)	Flight Lines	Height	GSD (cm)	Coverage (km ²)	Flight Lines
75	2	0.76	40	75	2	0.53	28
100	2.6	1.20	30	100	2.6	0.84	21
150	3.9	2.07	20	150	3.9	1.45	14
250	6.5	3.84	12	250	6.5	2.69	8
300	7.8	4.70	10	300	7.8	3.29	7

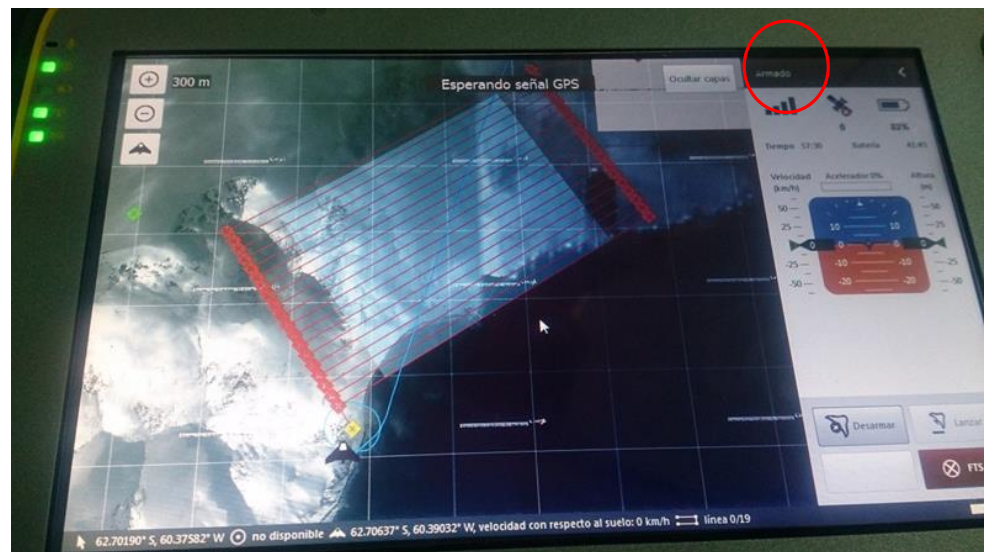


Figure 8. Planning the flight, using Trimble Access, over unexplored area U3 (see location in Figure 1). A communications failure is shown on the controller (icon within red circle).

- As mentioned in the Materials and Methods section, in general, the materials of the drone (main materials were high-density polyethylene foam, carbon frame structure and composite elements) were not affected by the low temperatures. This plane lands on its belly, so the structure is sufficiently reinforced to not suffer from landings, although there were some mishaps with bad landings that caused damage to the fuselage (see an illustration in [62]). This landing procedure applies except in the case of the shuttle (Figure 9). As was verified in Flight 4, when temperatures drop below $0\text{ }^{\circ}\text{C}$, the tension of the launcher tires decreases, which prevents the plane from taking off with sufficient speed. When launching the aircraft with its payload, the elastic band pushes the launch dock with more than $4g$ and with a speed of more than 60 km/h . As mentioned earlier, to maintain this performance below $0\text{ }^{\circ}\text{C}$ it is necessary to increase by at least 25% the standard elastic tension. To avoid this problem, the manufacturer recommends keeping the launcher as warm as possible and covering it immediately after the plane has been launched. An illustration of the tension of the shuttle tires at takeoff can be seen in [63].



Figure 9. Drone and shuttle at takeoff.

- Another problem due to the low temperatures at flight height was the icing of the aircraft wings. This mattered when flying in fog, as in the second flight of the first day. The mist of ice crystals in the fog suddenly lowered while the plane was in flight, causing the aircraft to fall. It was observed that the fuselage was frozen (e.g., Figure 10). The record of the black box was sent to the manufacturer to establish the reasons for the fall and they returned a report indicating that the plane suffered this sudden fall due to the freezing of the Pitot tube because of the low temperatures during the flight. The nearby fog on the first day of operation (Flight 1) can be appreciated in the video [64].



Figure 10. Example of icing on a drone wing (source: NASA [65]).

- The reflectivity of the snow was another variable that greatly conditioned the results obtained, due to its effects on the quality of the images taken. To reduce this problem, the camera settings had to be modified each day according to the existing lighting, as explained in the methods section. Even with these camera adjustments, when the data were processed, the point clouds obtained had many spikes due to the noise produced by snow reflectivity (Figure 11a). These were eliminated by applying filtering algorithms and point cloud classification to improve the results (Figure 11b).

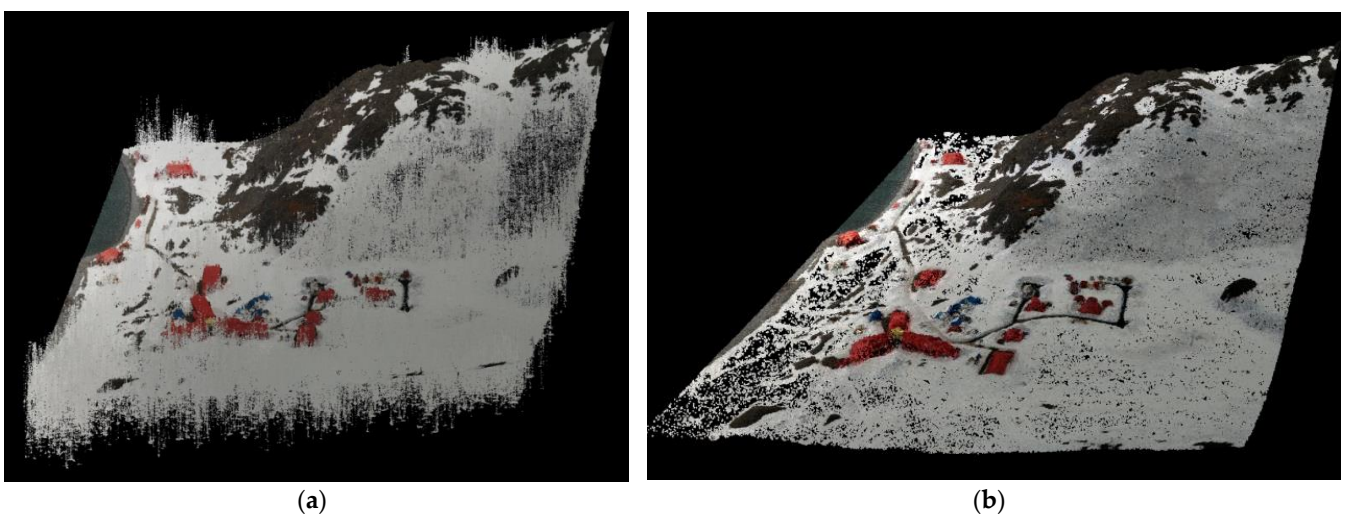


Figure 11. (a) Point cloud without filtering and (b) DSM obtained after filtering.

5. Regarding the aircraft's ability to reach remote areas, calculations were made to determine the area that could be covered by the flight and a safe position for the pilot to launch the drone. As shown in previous tables, and taking into account the battery reserve that had to be made to account for cold conditions, the entire planned remote area U3 (Figure 1), extending about 3 km², could have been covered using a flight height of 300 m. However, when the test flight was carried out, a loss of communication signal happened, which caused the UAS to make an emergency landing during flight F13 (Figure 8).

The DSM generated following the steps described in the methods section is the main final result, after its analysis and validation. The latter was done by comparing the Z coordinates of control points taken on the ground using differential GNSS techniques and the corresponding points extracted from the DSM (Table 8). The mean and standard deviation of the observed differences in absolute value were 0.16 ± 0.12 m, where the rather large standard deviation is due to two outliers (0.477 m and, to a lesser extent, 0.288 m), which we kept in the dataset to provide a real sense of the actual results.

Table 8. Differences between Z_GPS points and Z model points. X and Y are the UTM coordinates for sheet 33S.

Name	Y UTM (m)	X UTM (m)	Z GPS (m)	Z model (m)	Difference (m)
baejci_CGP01	3049294.639	633869.907	27.407	27.426	0.019
baejci_CGP02	3049295.409	633869.229	27.402	27.548	0.146
baejci_CGP03	3049296.854	633867.867	27.400	27.565	0.165
baejci_CGP04	3049294.801	633865.695	27.399	27.533	0.134
baejci_CGP05	3049361.754	633995.773	24.007	24.484	0.477
baejci_CGP06	3049344.414	633966.083	24.640	24.786	0.146
baejci_CGP07	3049344.271	633965.967	24.630	24.731	0.101
baejci_CGP08	3049353.455	633943.808	23.764	23.849	0.085
baejci_CGP09	3049352.922	633943.953	23.749	23.622	-0.127
baejci_CGP10	3049353.127	633944.669	23.751	23.633	-0.118
baejci_CGP12	3049341.692	633880.631	21.993	22.281	0.288

Other results of interest are the derived cartographies generated from these DSMs for use in different applications within glacier dynamics and mass balance studies. These derived maps include orthophotos (Figure 12a), contour maps (Figure 12b), orientation maps (Figure 12c), and slope maps (Figure 12d), which form part of the web publication of the results.

Once all the maps foreseen in the research objectives were generated, they were published on the web, as described in Section 3.7. They were generated locally through layers for each of the DSMs and derived maps, using the Geoserver software [50] and following the specifications of the OGC. The preview of the maps must be done with a GETMAP request to the WMS through a light client such as Leaflet or OpenLayers [59]. An example of the results of these publications is shown in Figure 13.

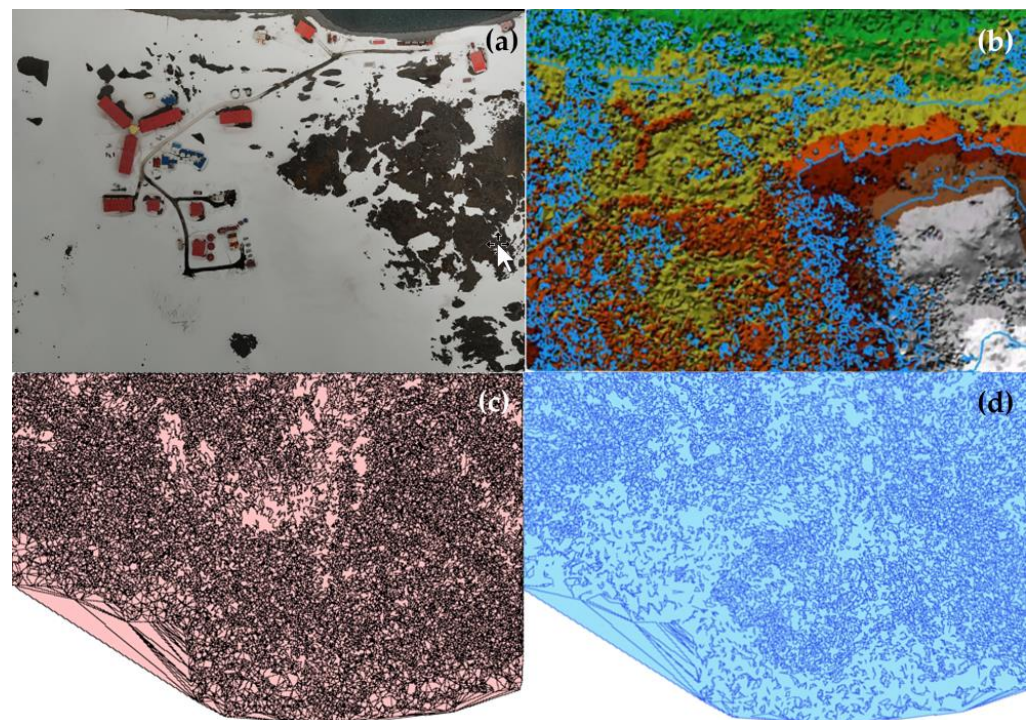


Figure 12. A sample of (a) orthophotos, (b) contour maps, (c) orientation maps, and (d) slope maps.

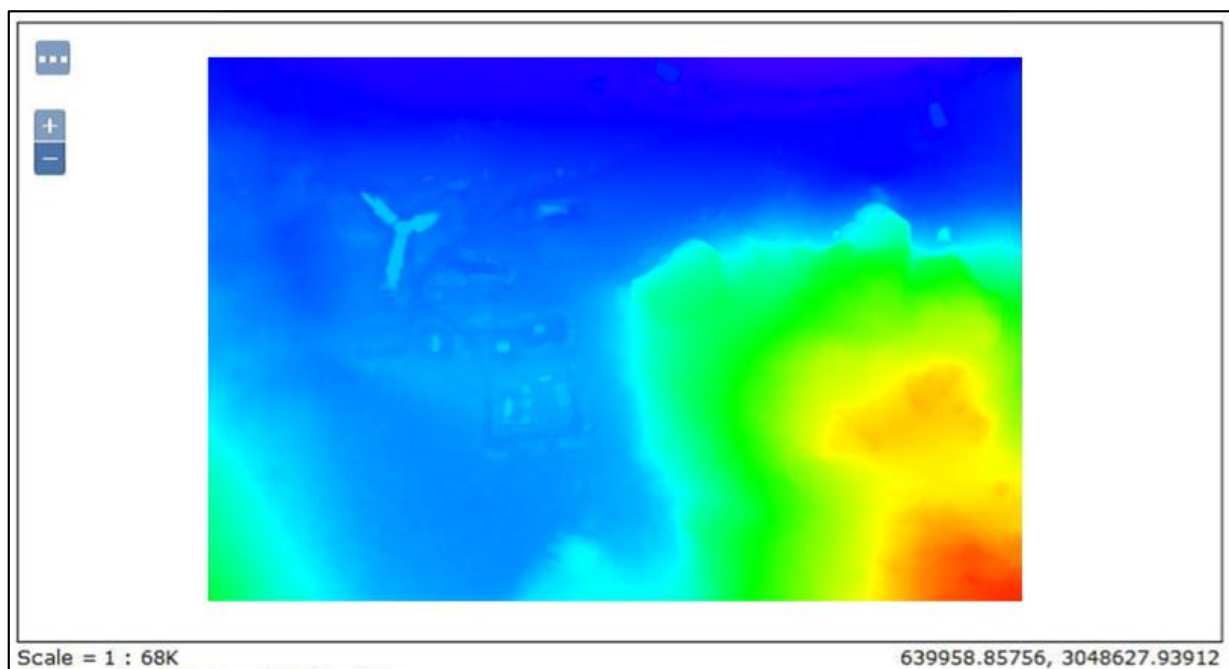


Figure 13. BAE JCI map visualized through OpenLayers. Colors represent the varying elevations, from lowest (darker blue) to highest (darkest red).

5. Discussion

Different hypotheses were raised in our investigation and tested through the case study. The behavior of the drone under the adverse weather conditions, available logistics, and amount of snow at the time of data collection confirmed that our commitment to fixed-wing RPAS was successful, although this does not preclude the use of multirotor systems. It is important to bear in mind that our case study was carried out using a Trimble UX5 RPAS with an electric engine (electric pusher propeller; brushless 700 W motor). There

is a significant difference in the ability to fly fixed-wing UAVs with combustion and electric propulsion. Other factors affecting flight efficiency are payload (batteries + task systems) and power requirements, which are different for either type of propulsion. The fixed-wing RPAS support high gusty winds and usually allow for a larger coverage of the area surveyed. Even so, we encountered many difficulties that were only partly mitigated by adapting the flight operations and the camera parameter configuration. The environmental difficulties included: (1) strong winds and gusts; (2) precipitation; (3) fog at low temperatures, which caused the icing of the drone's wings; (4) low temperatures that limited flight times because of its effect on reducing battery life; (5) strong reflectivity of the snow causing noise in the optical images. The main logistical difficulty was the access to the flight areas and working safely on them, due to the presence of crevasses. Both environmental and logistical difficulties implied a reduced number of days of flight.

Additional difficulties were encountered when using the available cartography for the terrain-exposed (nonglaciated) areas, as the existing cartography of the study area is from the 1990s (CGET map scale 1/25,000 [66]) and has not been updated. Moreover, this cartography was published with an error in the magnetic declination, due to a change in east–west orientation, which required the application of corresponding corrections.

Regarding the techniques of data processing, our results clearly show the interest of applying, to the point clouds obtained by photogrammetry, techniques such as segmentation and filtering, in order to allow for easier data handling and classification, and to eliminate the noise produced by the snow reflectivity.

One of the objectives set out in our study was the generation of precise models of the surface of the glaciers, which would improve the existing ones. The analysis of the generated maps, by comparing them with ground control points taken by means of GNSS techniques, indicates that the models have an accuracy of 0.16 ± 0.12 m in the vertical coordinate, which greatly improves that of the previously existing models. Although access to unmapped areas of these glaciers for modeling purposes was also initially considered, unfortunately, it was not possible to reach such unmapped areas due to limitations in the logistics available at the beginning of the Antarctic campaign.

In addition to its interest for glacier dynamics and mass balance studies, the DSMs obtained are useful for studies of safe transit areas over glaciers, mainly in zones close to the marine-terminating fronts, where large crevasses are frequent. The DSMs can also be used to track the advance and retreat of the glacier fronts.

As shown in the Results section, some flown glacier areas had no resolution in the image correlation, due to lack of contrast. The main reason was that, on the date of the flight, there was still a large amount of snow in the study area, so there were no rocky outcrops or differentiated elements on the glacier surface that could be identified in the photogrammetric process.

This leads us to consider, as a future line of research, the use of fixed-wing RPAS with airborne LiDAR (light detection and ranging, or laser imaging detection and ranging) sensors. This involves changing the data capture methodology from aerial photogrammetry to scanning of the glacier surface. LiDAR technology is less affected by the reflectivity of the snow, since it consists in the emission of a laser pulse that reflects off the ground and is measured again in the sensor. It allows the position of the points to be calculated directly, without requiring acquisition of aerial images and their subsequent processing. In this way, the noncorrelation of the images is avoided (or at least much minimized), and increased productivity is expected in the capture of the information, as no ground control points are needed. There are few case studies in Antarctica [21], so this is a field to explore that opens many possibilities.

Author Contributions: Conceptualization, A.B.B., F.N., A.Z. and M.Á.; methodology, A.B.B., A.Z. and M.Á.; software, A.B.B., M.M. and A.Z.; validation, F.N., J.R. and M.Á.; formal analysis, A.B.B. and M.M.; investigation, A.B.B., A.Z. and M.Á.; resources, A.B.B., A.Z. and M.Á.; data curation, A.B.B. and A.Z.; writing—original draft, A.B.B.; writing—review & editing, F.N., M.M. and M.Á.;

visualization, A.B.B.; supervision, F.N., J.R. and M.Á.; project administration, A.B.B., J.R. and M.Á.; funding acquisition, F.N. All authors have read and agreed to the published version of the manuscript.

Funding: This research was funded by grant PID2020-113051RB-C31 from Agencia Estatal de Investigación.

Data Availability Statement: The data are available from the Pangaea database <https://www.pangaea.de/>.

Acknowledgments: The authors thank the crew of Juan Carlos I Station for their logistical support.

Conflicts of Interest: The authors declare no conflict of interest.

References

1. Quincey, D.J.; Bishop, M.P.; Käab, A.; Berthier, E.; Flach, B.; Bolch, T.; Buchroithner, M.; Kamp, U.; Khalsa, S.J.S.; Toutin, T.; et al. Digital terrain modeling and glacier topographic characterization. In *Global Land Ice Measurements from Space*; Kargel, J.S., Ed.; Springer: Berlin/Heidelberg, Germany, 2014. [\[CrossRef\]](#)
2. Hodson, A.; Anesio, A.M.; Ng, F.; Watson, R.; Quirk, J.; Irvine-Fynn, T.; Dye, A.; Clark, C.; McCloy, P.; Kohler, J.; et al. Respires: Quantifying the distribution and respiration CO₂ flux of cryoconite across an entire Arctic supraglacial ecosystem. *J. Geophys. Res.-Biogeosciences* **2007**, *112*, wos000252014100001. [\[CrossRef\]](#)
3. Immerzeel, W.W.; Kraaijenbrink, P.D.A.; Shea, J.M.; Shrestha, A.B.; Pellicciotti, F.; Bierkens, M.F.P.; De Jong, S.M. High-resolution monitoring of Himalayan glacier dynamics using unmanned aerial vehicles. *Remote Sens. Environ.* **2014**, *150*, 93–103. [\[CrossRef\]](#)
4. Steiner, J.F.; Pellicciotti, F.; Buri, P.; Miles, E.S.; Immerzeel, W.W.; Reid, T.D. Modelling ice-cliff backwasting on a debris-covered glacier in the Nepalese Himalaya. *J. Glaciol.* **2015**, *61*, 889–907. [\[CrossRef\]](#)
5. Thakuri, S.; Khadka, D. Potentials and applications of unmanned aerial vehicles in environmental studies in Nepal: A review. *J. Nepal Sci. Olympiad.* **2016**, *1*, 31–40.
6. Fugazza, D.; Senese, A.; Azzoni, R.S.; Smiraglia, C.; Cernuschi, M.; Severi, D.; Diolaiuti, G.A. High-resolution mapping of glacier surface features. The UAV survey of the Forni Glacier (Stelvio National Park, Italy). *Geogr. Fis. E Din. Quat.* **2015**, *38*, 25–33. [\[CrossRef\]](#)
7. Turner, D.; Lucieer, A.; Watson, C. An Automated Technique for Generating Georectified Mosaics from Ultra-High Resolution Unmanned Aerial Vehicle (UAV) Imagery, Based on Structure from Motion (SfM) Point Clouds. *Remote. Sens.* **2012**, *4*, 1392–1410. [\[CrossRef\]](#)
8. Crocker, R.I.; Maslanik, J.A.; Adler, J.J.; Palo, S.E.; Herzfeld, U.C.; Emery, W.J. A Sensor Package for Ice Surface Observations Using Small Unmanned Aircraft Systems. *IEEE Trans. Geosci. Remote Sens.* **2011**, *50*, 1033–1047. [\[CrossRef\]](#)
9. Funaki, M.; Hirasawa, N.; Ant-Plane Group. Outline of a small unmanned aerial vehicle (Ant-Plane) designed for Antarctic research. *Polar Sci.* **2008**, *2*, 129–142. [\[CrossRef\]](#)
10. Funaki, M.; Higashino, S.-I.; Sakanaka, S.; Iwata, N.; Nakamura, N.; Hirasawa, N.; Obara, N.; Kuwabara, M. Small unmanned aerial vehicles for aeromagnetic surveys and their flights in the South Shetland Islands. *Antarctica. Polar Sci.* **2014**, *8*, 342–356. [\[CrossRef\]](#)
11. Turner, D.; Lucieer, A.; Malenovsky, Z.; King, D.H.; Robinson, S.A. Spatial Co-Registration of Ultra-High Resolution Visible, Multispectral and Thermal Images Acquired with a Micro-UAV over Antarctic Moss Beds. *Remote. Sens.* **2014**, *6*, 4003–4024. [\[CrossRef\]](#)
12. Gardner, S.; LeRoi, D.; Perryman, W. A penguin population polar express: NOAA's quest to count penguin breeds speeds up with a VTOL UAS. *Unmanned Syst.* **2011**, *29*, 30–35.
13. Lan, C.-T.E.; Keshmiri, S.; Hale, R. Fuzzy-Logic Modeling of a Rolling Unmanned Vehicle in Antarctica Wind Shear. *J. Guid. Control. Dyn.* **2012**, *35*, 1538–1547. [\[CrossRef\]](#)
14. Van den Kroonenberg, A.; Martin, T.; Buschmann, M.; Bange, J.; Vörsmann, P. Measuring the wind vector using the autonomous mini aerial vehicle M2AV. *J. Atmos. Oceanic Technol.* **2008**, *25*, 1969–1982. [\[CrossRef\]](#)
15. Wójcik-Długoborska, K.A.; Bialik, R.J. The Influence of Shadow Effects on the Spectral Characteristics of Glacial Meltwater. *Remote. Sens.* **2021**, *13*, 36. [\[CrossRef\]](#)
16. Pina, P.; Vieira, G. UAVs for Science in Antarctica. *Remote Sens.* **2022**, *14*, 1610. [\[CrossRef\]](#)
17. AMcKinnis, J.; LaGue, H.; Benyamen; Keshmiri, S. Dynamic Modeling and Flight Test Validation of an In-House Design UAS Built for Polar Research. In Proceedings of the 2020 IEEE Aerospace Conference, Big Sky, MT, USA, 7–14 March 2020; pp. 1–7. [\[CrossRef\]](#)
18. Rodzewicz, M.; Goraj, Z.; Tomaszewski, A. Design and testing of three tailless unmanned aerial vehicle configurations built for surveillance in Antarctic environment. *Proc. Inst. Mech. Eng. Part G J. Aerosp. Eng.* **2018**, *232*, 2598–2614. [\[CrossRef\]](#)
19. Sheridan, I. Drones and global navigation satellite systems: Current evidence from polar scientists. *R. Soc. Open Sci.* **2020**, *7*, 191494. [\[CrossRef\]](#) [\[PubMed\]](#)
20. Bollard, B.; Doshi, A.; Gilbert, N.; Poirot, C.; Gillman, L. Drone Technology for Monitoring Protected Areas in Remote and Fragile Environments. *Drones* **2022**, *6*, 42. [\[CrossRef\]](#)

21. Li, T.; Zhang, B.; Xiao, W.; Cheng, X.; Li, Z.; Zhao, J. UAV-Based Photogrammetry and LiDAR for the Characterization of Ice Morphology Evolution. *IEEE J. Sel. Top. Appl. Earth Obs. Remote Sens.* **2020**, *13*, 4188–4199. [CrossRef]
22. Václav, P.; Barták, M. Multispectral aerial monitoring of a patchy vegetation oasis composed of different vegetation classes. UAV-based study exploiting spectral reflectance indices. *Czech Polar Rep.* **2022**, *12*, 131–142. [CrossRef]
23. Malenovský, Z.; Lucieer, A.; King, D.H.; Turnbull, J.D.; Robinson, S.A. Unmanned aircraft system advances health mapping of fragile polar vegetation. *Methods Ecol. Evol.* **2017**, *8*, 1842–1857. [CrossRef]
24. Turner, D.; Lucieer, A.; Malenovský, Z.; King, D.; Robinson, S.A. Assessment of Antarctic moss health from multi-sensor UAS imagery with Random Forest Modelling. *Int. J. Appl. Earth Obs.* **2018**, *68*, 168–179. [CrossRef]
25. Shah, K.; Ballard, G.; Schmidt, A.; Schwager, M. Multidrone aerial surveys of penguin colonies in Antarctica. *Sci. Robot.* **2020**, *5*, eabc3000. [CrossRef]
26. Tan, A.E.-C.; McCulloch, J.; Rack, W.; Platt, I.; Woodhead, I. Radar Measurements of Snow Depth Over Sea Ice on an Unmanned Aerial Vehicle. *IEEE Trans. Geosci. Remote Sens.* **2020**, *59*, 1868–1875. [CrossRef]
27. Liu, E.J.; Wood, K.; Aiuppa, A.; Giudice, G.; Bitteto, M.; Fischer, T.P.; Kilbride, B.T.M.; Plank, T.; Hart, T. Volcanic activity and gas emissions along the South Sandwich Arc. *Bull. Volcanol.* **2021**, *83*, 3. [CrossRef]
28. Fudala, K.; Bialik, R.J. The use of drone-based aerial photogrammetry in population monitoring of Southern Giant Petrels in ASMA 1, King George Island, maritime Antarctica. *Glob. Ecol. Conserv.* **2021**, *33*, e01990. [CrossRef]
29. Hinke, J.T.; Giuseffi, L.M.; Hermanson, V.R.; Woodman, S.M.; Krause, D.J. Evaluating Thermal and Color Sensors for Automating Detection of Penguins and Pinnipeds in Images Collected with an Unoccupied Aerial System. *Drones* **2022**, *6*, 255. [CrossRef]
30. Zmarz, A.; Rodzewicz, M.; Dąbski, M.; Karsznia, I.; Korczak-Abshire, M.; Chwedorzewska, K. Application of UAV BVLOS remote sensing data for multi-faceted analysis of Antarctic ecosystem. *Remote Sens. Environ.* **2018**, *217*, 375–388. [CrossRef]
31. Kung, O.; Strecha, C.; Beyeler, A.; Zufferey, J.C.; Floreano, D.; Fua, P.; Gervais, F. The Accuracy of Automatic Photogrammetric Techniques on Ultra-Light Uav Imagery. In Proceedings of the UAV-g 2011—Unmanned Aerial Vehicle in Geomatics, Zürich, Switzerland, 14–16 September 2011.
32. Open Geospatial Consortium (OGC). Available online: <https://www.ogc.org> (accessed on 12 March 2022).
33. Infraestructura de Datos Espaciales Española (IDEE). Available online: <http://www.idee.es> (accessed on 12 March 2022).
34. Directiva Europea INSPIRE. Available online: <https://inspire.ec.europa.eu> (accessed on 12 March 2022).
35. Organización Internacional de Estandarización. Available online: <https://www.iso.org/home.html> (accessed on 12 March 2022).
36. Bañón, M.; Vasallo, F. *AEMET en la Antártida. Climatología y Meteorología Sinóptica en la Estaciones Meteorológicas Españolas en la Antártida*; AEMET: Madrid, Spain, 2015.
37. Brezoescu, A.; Castillo, P.; Lozano, R. Straight-Line Path Following in Windy Conditions. *ISPRS-Int. Arch. Photogramm. Remote Sens. Spat. Inf. Sci.* **2012**, XXXVIII-1, 283–288. [CrossRef]
38. Watts, A.C. Ambrosia, Vincent G. Hinkley, Everett A. Unmanned Aircraft Systems in Remote Sensing and Scientific Research: Classification and Considerations of Use. *Remote Sens.* **2012**, *4*, 2072–4292. [CrossRef]
39. Barton, J.D. Fundamentals of Small Unmanned Aircraft Flight. *Johns Hopkins APL Tech. Dig.* **2012**, *21*, 132–149.
40. Trimble UAV UX5. Available online: <https://geotronics.es/productos/aeronaves-no-tripuladas/trimble-ux5> (accessed on 12 March 2022).
41. Camera Sony NEX-5. Available online: <https://www.sony.es/electronics/support/res/manuals/4437/44370084M.pdf> (accessed on 12 March 2022).
42. Trimble UX5 User Guide. Available online: https://help.trimblegeospatial.com/TALegacy/Help%20Files/AI_2_0/Espanol/UX5AerialImagingUserGuide.pdf (accessed on 12 March 2022).
43. Torno, C.; Hintz, C.; Carrillo, L.R.G. Design and Development of a Semi-Autonomous Fixed-Wing Aircraft with Real-Time Video Feed. In Proceedings of the International Conference on Unmanned Aircraft Systems (ICUAS), Orlando, FL, USA, 27–30 May 2014; pp. 1021–1028. [CrossRef]
44. Dumont, M.; Arnaud, Y.; Six, D.; Corripio, J.G. Retrieval of glacier surface albedo using terrestrial photography. *Houille Blanche-Rev. Int. De L Eau.* **2009**, *2*, 102–108. [CrossRef]
45. Trimble Access Aerial Imaging. Available online: <https://apps.trimbleaccess.com/help/en/AerialImaging=2.2.6> (accessed on 12 March 2022).
46. Trimble. Available online: <https://www.trimble.com> (accessed on 12 March 2022).
47. Trimble Business Center (TBC). Photogrammetry Module. White Paper. 2013. Available online: https://www.cansel.ca/store/_ui/responsive/theme-cansel/pdf/canselContent/Trimble-Business-Center-Photogrammetry-Module-White-Paper-English.pdf (accessed on 12 March 2022).
48. ESRI España. Available online: <https://www.esri.es/es-es/arcgis/sobre-arcgis/introduccion> (accessed on 12 March 2022).
49. PostGIS Spatial and Geographic Objects for PostgreSQL. Available online: <https://postgis.net> (accessed on 12 March 2022).
50. GeoServer. Available online: <http://geoserver.org> (accessed on 12 March 2022).
51. Youtube Video (by the Authors). Available online: https://youtu.be/Ymxtm6uv_Ec (accessed on 3 November 2022).
52. López-Cuervo Medina, S. *Apuntes de Fotogrametría Digital*; Universidad Politécnica de Madrid, Fotogrametría: Madrid, Spain, 1980; ISBN 84-3000-2559-6.
53. Software GRASS. Available online: <https://grass.osgeo.org> (accessed on 12 March 2022).

54. Cerro, G. Estudio y Comparativa de Algoritmos de Modelado 3D en Software Libre y Propietario para el Desarrollo de un Prototipo de una IDE de la Antártida. Master Thesis, Universidad Politécnica de Madrid, Madrid, Spain, 2020.
55. Cloud Optimized GeoTIF. Available online: <https://www.cogeo.org/> (accessed on 12 March 2022).
56. Sierra, A. GeoJSON y TopoJSON: Comparación Entre los Formatos de Intercambio de Información Geográfica Alternativos a GML. In Proceedings of the IV Jornadas Ibéricas de Infraestructura de Datos Espaciales, Toledo, Spain, 13–15 November 2013.
57. 13LandXML. Available online: <https://www.landxml.org> (accessed on 12 March 2022).
58. Sterling, J. *The History and Importance of Web Mapping*; College of Earth and Mineral Sciences, The Pennsylvania State University: State College, PA, USA, 2017.
59. OpenLayers. Available online: <https://openlayers.org> (accessed on 12 March 2022).
60. Youtube Video (by the Authors). Available online: <https://youtu.be/9vMfRgaEy48> (accessed on 3 November 2022).
61. YouTube Video (Noticias Cuatro, 21/12/2014). Available online: <https://youtu.be/SGOq3JtO1C8> (accessed on 3 November 2022).
62. Youtube Video (by the Authors). Available online: <https://youtu.be/Bg3YP6harDk> (accessed on 3 November 2022).
63. Youtube Video (by the Authors). Available online: https://youtu.be/GEdMn_JegI8 (accessed on 3 November 2022).
64. Youtube Video (by the Authors). Available online: <https://youtube.com/watch?v=Jy0ugcvqgik&feature=share> (accessed on 3 November 2022).
65. NASA. Available online: https://spinoff.nasa.gov/Spinoff2011/ps_2.html (accessed on 12 March 2022).
66. Centro Geográfico del Ejército de Tierra Español (CGET). Available online: <https://ejercito.defensa.gob.es/unidades/Madrid/ceget> (accessed on 12 March 2022).